Convergence of melt electrowriting and extrusion-based bioprinting for vascular patterning of a myocardial construct

DOI:
[10.1088/1758-5090/ace07f](10.1088/1758-5090/ace07f)

Document status and date:
Published: 01/07/2023

Document Version:
Publisher's PDF, also known as Version of Record (includes final page, issue and volume numbers)

Please check the document version of this publication:

• A submitted manuscript is the version of the article upon submission and before peer-review. There can be important differences between the submitted version and the official published version of record. People interested in the research are advised to contact the author for the final version of the publication, or visit the DOI to the publisher's website.
• The final author version and the galley proof are versions of the publication after peer review.
• The final published version features the final layout of the paper including the volume, issue and page numbers.

Link to publication

PAPER • OPEN ACCESS

Convergence of melt electrowriting and extrusion-based bioprinting for vascular patterning of a myocardial construct

To cite this article: Madison Jade Ainsworth *et al* 2023 *Biofabrication* **15** 035025

View the article online for updates and enhancements.

Biofabrication

PAPER

Convergence of melt electrowriting and extrusion-based bioprinting for vascular patterning of a myocardial construct

Madison Jade Ainsworth[1,2,8] ⓘ, Nino Chirico[2,3,4,8] ⓘ, Mylène de Ruijter[1,2] ⓘ, Andrei Hrynevich[1,2,5],
Inge Dokter[2,3,4], Joost P G Sluijter[2,3,4] ⓘ, Jos Malda[1,2,5] ⓘ, Alain van Mil[2,3,4,9] ⓘ and Miguel Castilho[1,6,7,9,*] ⓘ

1 Department of Orthopedics, University Medical Center Utrecht, Utrecht, The Netherlands
2 Regenerative Medicine Center Utrecht, University Medical Center Utrecht, Utrecht University, Utrecht, The Netherlands
3 Department of Cardiology, Experimental Cardiology Laboratory, University Medical Center Utrecht, Utrecht, The Netherlands
4 Circulatory Health Research Center, University Medical Center Utrecht, Utrecht, The Netherlands
5 Department of Clinical Sciences, Faculty of Veterinary Sciences, Utrecht University, Utrecht, The Netherlands
6 Department of Biomedical Engineering, Eindhoven University of Technology, Eindhoven, The Netherlands
7 Institute for Complex Molecular Systems, Eindhoven University of Technology, Eindhoven, The Netherlands
* Author to whom any correspondence should be addressed.
8 Shared first authors
9 Shared senior authors

E-mail: m.dias.castilho@tue.nl

Abstract

To progress cardiac tissue engineering strategies closer to the clinic, thicker constructs are required to meet the functional need following a cardiac event. Consequently, pre-vascularization of these constructs needs to be investigated to ensure survival and optimal performance of implantable engineered heart tissue. The aim of this research is to investigate the potential of combining extrusion-based bioprinting (EBB) and melt electrowriting for the fabrication of a myocardial construct with a precisely patterned pre-vascular pathway. Gelatin methacryloyl (GelMA) was investigated as a base hydrogel for the respective myocardial and vascular bioinks with collagen, Matrigel and fibrinogen as interpenetrating polymers to support myocardial functionality. Subsequently, extrusion-based printability and viability were investigated to determine the optimal processing parameters for printing into melt electrowritten meshes. Finally, an anatomically inspired vascular pathway was implemented in a dual EBB set-up into melt electrowritten meshes, creating a patterned pre-vascularized myocardial construct. It was determined that a blend of 5% GelMA and 0.8 mg·ml^{-1} collagen with a low crosslinked density was optimal for myocardial cellular arrangement and alignment within the constructs. For the vascular fraction, the optimized formulation consisted of 5% GelMA, 0.8 mg·ml^{-1} collagen and 1 mg·ml^{-1} fibrinogen with a higher crosslinked density, which led to enhanced vascular cell connectivity. Printability assessment confirmed that the optimized bioinks could effectively fill the microfiber mesh while supporting cell viability ($\sim$70%). Finally, the two bioinks were applied using a dual EBB system for the fabrication of a pre-vascular pathway with the shape of a left anterior descending artery within a myocardial construct, whereby the distinct cell populations could be visualized in their respective patterns up to D14. This research investigated the first step towards developing a thick engineered cardiac tissue construct in which a pre-vascularization pathway is fabricated within a myocardial construct.

1. Introduction

Heart failure is a leading cause of morbidity and mortality, with a prevalence of 64 million cases worldwide [1]. Heart failure with a reduced ejection fraction is typically associated with a primary myocardial injury like myocardial infarction, resulting in the loss of up to a billion cardiomyocytes with subsequent

scar formation and functional decline occurring. The heart has an extremely limited capacity to form new cardiomyocytes and regenerate itself [2, 3], therefore despite major advances in surgical and pharmaceutical treatments, the only curative treatment for heart failure is heart transplantation (HTx). However, due to HTx associated complications and donor availability limitations, regenerative medicine is seen as a potential strategy for a cure for heart diseases. Several new regenerative strategies have been tested and developed since the 2000s [4], ranging from direct single-cell injection, limited by cellular retention [5], towards external application of engineered cardiac tissues, bypassing retention issues [6]. Nevertheless, the strong need exists for further developments of engineering techniques [7]. To overcome high hemodynamic and mechanical stresses in the heart, engineered heart tissues (EHTs) have been improved by using scaffolds that provide mechanical stability and guide anisotropic cell alignment by mimicking the native extracellular matrix (ECM) [8–10].

The more advanced EHTs typically comprise a biocompatible scaffold and an ECM-like hydrogel with embedded cells [11]. Previously, we have shown that well-ordered, fiber scaffolds with hexagonal microarchitectures obtained by a fiber patterning method called melt electrowriting (MEW) could support contracting human induced pluripotent stem cell-derived cardiomyocytes (iPSC-CMs) and direct their maturation, alignment and anisotropic ECM organization *in vitro* [10]. Although promising, the currently generated EHT thickness (approximately 400 μm) still needs further developments to enable force-generation and improve *in vivo* myocardial functionality, which may be achieved through the generation of thicker cell-laden EHTs. Prior to generating thicker EHTs, the anastomotic connection of cardiac constructs with the host is a major goal for effective clinical translation; *in vivo* studies proved that pre-vascularizing constructs ensures functional vessel connection upon implantation, as well as enhancing perfusion, integration and ultimately, implantation success of the cardiac constructs [12, 13].

To potentially overcome these limitations, we further developed a concept of combining MEW with extrusion-based bioprinting (EBB) to incorporate a patterned pre-vascular network within EHTs. EBB has been commonly used for the controlled spatial deposition of different cell types and/or biomolecules [14] and has been applied to endothelial cells, cardiomyocytes and other cardiac cell sub-populations [15–17], which are encapsulated in a (bio)polymer gel, together referred to as a bioink. Convergence of additive manufacturing and biofabrication technologies allows for the combined advantages of the individual processes [18, 19]. For example, it was shown that the combination of EBB and MEW within the same process allowed for controlled hydrogel deposition within microfiber constructs [14, 20]. Additionally, the convergence of these two technologies allows for reinforcement of hydrogels to improve the global mechanical properties [21, 22]. To the authors' knowledge, the combination of EBB with MEW has not yet been explored for the application of creating a pre-vascular pathway within a myocardial construct.

Building on this evidence, we hypothesized that by using a converged printing approach of MEW and EBB, we can create a bioengineered myocardial construct that includes a pre-vascular network. Such constructs will induce anisotropic ECM organization and cellular alignment through the use of well-organized microfiber scaffolds and a precisely patterned pre-vascular path. To test this hypothesis, myocardial and vascular bioinks were first designed and investigated for biological function and subsequently EBB potential. The myocardial bioink based on GelMA was optimized with interpenetrating polymers (collagen and Matrigel) to facilitate the maturation and functionality of cardiac cells, allowing for native matrix production and the formation of tissue-like structures, while the vascular bioink, based on GelMA, collagen and fibrinogen, was investigated on photoinitiator concentration with consequent crosslinked density to support the formation of endothelial/capillary networks. These gels were then tested for suitability for EBB as well as MEW mesh infiltration using the converged EBB and MEW printing approach. Viability of the respective cell populations in their optimized bioink was also investigated before using a dual-EBB approach to fabricate a pre-vascularized patterned myocardial construct. In summary, this study shows the findings and future steps of the development and evaluation of a myocardial construct with a vascular pattern through convergence of EBB and MEW, with the aim of providing a platform for anisotropic cellular alignment (contractive tissue formation) and patterned pre-vascularization (to enable future anastomosis with the host). Furthermore, this platform could overcome the diffusion limit that hinders the generation of thicker EHTs to meet functional requirements.

2. Materials and methods

2.1. Cell culture

2.1.1. Human iPSC culture and cardiomyocyte differentiation
Three healthy human peripheral blood mononuclear cell (PBMC)-derived iPSC lines were used: UKKi032-C (NP0141-31B) [23] and UKKi036-C (NP0143-18), females and UKKi037-C (NP0144-41, male) [23]. All cell lines have previously been deposited in the European Bank for induced pluripotent Stem Cells (EBiSC, https://ebisc.org/) and are registered in the online registry for human pluripotent stem cell lines

Table 1. Myocardial and vascular bioink hydrogel candidates for evaluation.

	Name	Base hydrogel	Interpenetrating polymers	Photoinitiator concentration (Ru/SPS) (mM)
Myocardial hydrogel candidates	GelMA	5% w/v GelMA	—	0.25/2.5
	GelMA-collagen	5% w/v GelMA	0.8 mg·ml^{-1} collagen (rat tail)	0.25/2.5
	GelMA-matrigel	5% w/v GelMA	1 mg·ml^{-1} Matrigel	0.25/2.5
Vascular hydrogel candidates	Vasc_B Stiff	5% w/v GelMA	0.8 mg·ml^{-1} collagen (rat tail) and 1 mg·ml^{-1} fibrinogen	0.5/5
	Vasc_B Soft	5% w/v GelMA		0.25/2.5

(hPSCreg, https://hpscreg.eu/). The study met the criteria of the code of proper use of human material according to international guidelines. iPSCs were cultured (passage 29–44) and differentiated into CMs using a GiWi differentiation protocol as described previously [24]. iPSC-CMs were used in experiments on D21-22.

2.1.2. Primary cell culture: human fetal cardiac fibroblasts

Isolation of human fetal cardiac fibroblasts hfCFs was performed as described previously [25, 26] following parental permission using standard informed consent procedures and approval by the ethics committees of the University Medical Center Utrecht and Leiden University Medical Center, the Netherlands. This is in accordance with the principles outlined in the Declaration of Helsinki [27]. hfCFs were cultured in hfCFb culture media (supplementary table 2). hfCFs were cultured to passage 7–10 for experimental use.

2.1.3. Primary cell culture: human umbilical vein endothelial cells (HUVECs)

Primary HUVECs were purchased from Lonza and maintained in EGM™-2 Endothelial Cell Growth Medium-2 (supplementary table 2) and cultured according to company instructions. HUVECs used were passage 6–7 for experiments in this study.

2.2. Myocardial and vascular bioinks

Three different hydrogels were evaluated as possible candidates for myocardial bioink and two for the vasculature part (table 1). All hydrogels contained GelMA (made from porcine gelatin type A, 175 bloom, 80% degree of functionalization (DoF), Sigma-Aldrich; and functionalized with methacrylic anhydride, Sigma-Aldrich) [28] as the base network and type 1 rat tail collagen (RatCol®), fibrinogen (Sigma-Aldrich, F8630) or Matrigel (Corning, 356231) as interpenetrating polymers. GelMA alone was also investigated. Hydrogel blends were supplemented with tris(2,2′-bipyridyl)dichlororuthenium (II) hexahydrate (Ru, Sigma-Aldrich) and sodium persulfate (SPS, Sigma-Aldrich) as photo-initiators. Crosslinking reaction was initiated via white light

Table 2. Construct's cellular composition.

Hydrogel	Cellular composition	Ratio	Cell density (cells ml^{-1})
Myocardial	iPSC-CM + hfCF	9:1	6×10^7
Vascular	HUVECs + hfCFs	5:1	3×10^7

(floodlight) and subsequentially, the system was incubated at 37 °C to allow for thermal crosslinking of collagen and Matrigel.

2.3. *In vitro* constructs

Initially, we proceeded with optimizing the cellular composition of the EHT. Constructs were prepared with iPSC-CMs alone (CMs only), co-culture of iPSC-CMs and hfCFs (CMs + FBs), as well as iPSC-CMs, hfCFs and HUVEC without patterning (CMs + FBs + ECs). The co-culture condition (CMs + FBs) was selected for further studies. Further details are reported in the supplementary information section.

2.3.1. Preparation of in vitro constructs

Cell suspensions (table 2) were spun down at $300 \times$ g for 3 min, then resuspended in the respective hydrogel solution. The 40 μl bioink (cell-hydrogel mix) was casted inside a hexagonal mesh (⌀8 mm discs) on a Teflon mold using a positive displacement pipette (Pos-D™ positive-displacement pipette, Mettler Toldedo). The Ru/SPS crosslinking was initiated by exposing the constructs to white light (floodlight) for 4 min. Subsequently, the system was incubated at 37 °C for collagen/Matrigel crosslinking for 12 min. Following gelation, constructs were transferred into a 24-well suspension plate containing 2 ml of pre-warmed (37 °C) Construct Medium (supplementary table 2). After one hour, the medium was changed to remove the excess photoinitiator. The 1.5 ml of medium was changed every other day.

2.3.2. Outputs
2.3.2.1. Beating rate and contraction analysis
Videos were taken using a GoPro Black Hero 7 camera connected to a bright field microscope via c-mount

system. Twenty second videos were taken at D14 and D21, and beating rate was manually calculated.

2.3.2.2. Immunofluorescent labeling

For immunofluorescent labeling experiments, constructs were fixed using 4% paraformaldehyde at room temperature for 20 min. After washing with Dulbecco's phosphate-buffered saline (DPBS; Gibco), cells were permeabilized using 0.1% Triton-X-100 (Sigma-Aldrich) at room temperature for 20 min and blocked in 10% goat serum (Sigma-Aldrich) at room temperature for 40 min. Next, primary antibodies (see supplementary table 3) diluted in DPBS were added and incubated at 4 °C overnight. The myocardial constructs were stained for vimentin, cardiac troponin T, and Hoechst. The vascular constructs were stained for CD31, vimentin, αSMA, and Hoechst (see supplementary table 3 for detailed antibody information). Secondary labeling was achieved by appropriate Alexa fluor antibodies (see supplementary table 3), and Hoechst diluted in DPBS at room temperature for 4 h. Images were taken using a Leica Thunder microscope (Leica) and processed using Thunder instant computational clearing at 70% strength.

2.3.2.3. Live cell labeling for vascular network assessment

Commercially available long-chain dialkylcarbocyanines (Invitrogen™ Vybrant™ Multicolor Cell-Labeling Kit (DiO, DiD)) were used to label HUVECs and hfCFs, respectively. Cells were trypsinized shortly before gel encapsulation, then cell-labeling solutions were added to culture medium (5 μl per million cells) and incubated for 30 min at 37 °C. Unbound cell-labeling solution was removed by spinning down, washing, and resuspending the pellet in fresh medium according to manufacturer guidelines. Medium was changed every other day. Samples were imaged using a Leica Thunder microscope (Leica) at D3, D7, D10 and processed using Thunder instant computational clearing at 70% strength. Network formation was quantified using the Angiogenesis Analyzer tool on FIJI (FIJI is Just ImageJ, NIH) software, as described [29] and demonstrated (supplementary figure 1).

2.3.2.4. Live/dead staining for bioprinting viability

Cast and bioprinted samples were collected on D1 and D7 for viability analysis using a live and dead staining. Calcein-AM (Invitrogen) was used to stain live cells and ethidium homodimer-1 (Invitrogen) was used to stain dead cells according to the manufacturer's protocol. Samples were imaged using a Leica Thunder microscope (Leica) and processed using Thunder instant computational clearing at 70% strength.

2.3.2.5. Cellular metabolic activity

On D1, D3 and D7, cellular metabolic activity was evaluated via alamarBlue Cell Viability Assay (Thermo Fisher Scientific). Hydrogels ($n = 4$) were incubated at 37 °C for 4 h in alamarBlue solution (10% v·v^{-1}) in Construct Medium. Then, the solution was plated out in triplicate prior to reading fluorescence using excitation/emission of 544/670 using a fluorescent microplate reader Fluoroskan Ascent FL (Thermo Fisher Scientific). Fluorescent values minus blank solution were normalized to casted samples as a comparative percentage.

2.4. Hydrogel material characterization

2.4.1. Sol-fraction and swelling analysis

Candidate hydrogels were characterized using soluble fraction and mass swelling ratio analyses to compare to *in vitro* results. Hydrogels were prepared by casting discs ($\emptyset = 6$ mm) using a custom-made Teflon mold ($n = 6$ per gel candidate).

Sol-fraction was defined by the percentage of mass loss, indicating the uncrosslinked macromers in the hydrogel network after exposure to light. It was calculated using:

$$\text{sol fraction} = \frac{(m_{\text{dry}, t0} - m_{\text{dry}, t1})}{m_{\text{dry}, t1}} \times 100\%. \quad (1)$$

The mass swelling ratio is indicated by the liquid volume of the constructs and was calculated using:

$$q = \frac{m_{\text{swollen}, t1}}{m_{\text{dry}, t1}}. \quad (2)$$

2.4.2. Rheological measurements

Rheology was performed on the hydrogel candidates to identify shear-thinning properties and viscosity. Rheology was performed at 10 °C, 12.5 °C and 15 °C using a Hybrid Rheometer (HR-2 Discovery, TA Instruments) equipped with a 20 mm flat plate geometry. Parameters used for amplitude sweeps were 1%–1000% strain with 5 points per decade at 10 rad s^{-1} angular frequency, and for frequency sweeps were 100–0.1 rad s^{-1} angular frequency with 5 points per decade at 5% strain and 1 Hz frequency ($n = 3$ for each temperature). The storage modulus (G'), loss modulus (G''), complex viscosity (η) and tanδ were recorded. Yield stress was defined as the crossover point between G' and G'', determined using TRIOS software version 5.1 (TA Instruments).

2.5. Melt electrowriting (MEW)

Melt electrowritten microfiber meshes were fabricated as previously described [10]. Briefly, a multitool 3D printer (3DDiscovery evolution, regenHU) was used to fabricate hexagonal-geometry MEW meshes with a side length of 400 μm using medical-grade poly-e-caprolactone (PCL; Purasorb, Corbion). The polymer granules were loaded into a syringe and melted to 80 °C before being extruded through a 24 G needle using 1.4 bar pressure. A Taylor cone was established using 7 kV acceleration voltage with

a 4 mm tip-collector distance, and fibers were collected at 8 mm s^{-1} (defined as the critical translation speed). Constructs were printed with 20 layers with fiber $\varnothing \approx 10.94 \pm 1.44\ \mu$m, resulting to a total scaffold thickness of $\sim$400 μm due to overlapping segments of the g-code (supplementary figure 2). For hydrogel-mesh integration analysis and pre-vascularized EHTs, samples were prepared as a 12 × 12 mm square for subsequent gel infiltration. For *in vitro* experiments, larger mesh sheets (approx. 50 × 50 mm) were sectioned using an $\varnothing = 8$ mm biopsy punch. Constructs were then sterilized using UV-light for 20 min per side.

2.6. Bioink printability and mesh integration
To assess the bioink's printability, the hydrogels were characterized by EBB parameter sweeps, assessing filament diameter and inter-filament spacing. Secondly, the parameters were investigated for integration within the MEW mesh. Finally, the filling of the meshes with the bioinks was investigated. All EBB experiments were carried out using a 23-gauge needle with a length of 9 mm.

2.6.1. Printability measurements
Standardized hydrogel printability assessments using extrusion based bioprinting were carried out (supplementary figures 3(A) and (B)) [30]. Firstly, fiber diameter measurements were made of each gel at 10 °C, 12.5 °C and 15 °C using the minimum extrusion pressure. Filament fusion tests, as previously described [30], were additionally performed using intervals from 3 to 0.45 mm.

2.6.2. Mesh integration measurements
Candidate hydrogels were extruded directly above the previously printed MEW meshes. The needle was positioned to a working distance of 0 μm, determined using a microscope camera within the printer, and the filling of the hexagonal microarchitectures with the hydrogels was examined (supplementary figure 5). The g-code was designed so that the path of the printhead would transect every 2nd row of hexagonal pores in the longest axis of the hexagons. Measurements were made of each gel at 10 °C, 12.5 °C and 15 °C using the minimum extrusion pressure (for continuous extrusion). Analysis was performed by calculating a percentage of filled hexagonal pores against the total number of pores in the programmed path (figure 3(B)), $n = 3$.

2.6.3. Mesh filling assessment
Filling of the entire mesh using a g-code transecting every adjacent row of hexagons (figure 3(E)) was performed and visualization of the whole construct was performed using brightfield microscopy tile scanning (Leica). Filling experiments were carried out using 1

layer (1L; $n \geqslant 3$) and 3 layers (3L; $n = 3$) of the g-code for each of the candidate hydrogels at 15 °C.

2.7. Converged MEW and dual-bioprinting system
2.7.1. Defining the anatomical vascular pathway and the dual EBB g-code
A selection was made from a coronary angiogram of a segment of the left anterior descending (LAD) artery, provided by Dr C. Hacking [31]. The image was then thresholded using ImageJ to define the vascular pathway. The pathway was overlayed with the hexagonal g-coded path and the dual-EBB g-code was prepared based on the filament distance of $1/2 \times$ hexagonal height.

2.7.2. Dual hydrogel extrusion setup
The MEW hexagonal scaffolds were printed as described in 2.1 and retained on the glass slide inside the sterile biosafety cabinet that houses the bioprinter (3DDiscovery Evolution, RegenHU). The scaffolds were subsequently sterilized for 30 min using UV light. Once each respective bioink was prepared according to the previously mentioned compositions, the bioinks were transferred to clear cartridges and placed inside the 3DDiscovery. Each subsequent hydrogel was cooled to 15 °C for 5 min using the cartridge cooler (Huber) prior to extrusion. The two bioinks were extruded subsequently according to the predefined anatomical pathway of the LAD artery, using the optimized EBB parameters.

2.8. Statistical analysis
All statistical analysis was performed in Graphpad Prism v9.4.1. Two-way analysis of variance (ANOVA) analysis with Tukey's multiple comparison was carried out for all analysis unless otherwise stated. Statistical analysis of printing optimization was performed using a Kruskal Wallis test using Dunn's multiple comparison analysis to compare between printing temperatures of each gel candidate. *P*-values are denoted according to the following: (n.s.) $p > 0.05$, (*) $p \leqslant 0.05$, (**) $p \leqslant 0.01$, (***) $p \leqslant 0.001$, (****) $p \leqslant 0.0001$. Differences were considered statistically significant when $p < 0.05$.

3. Results

3.1. Myocardial and vascular bioinks optimization and characterization
Three myocardial bioink candidates were examined for tissue-like formation using a co-culture of iPSC-CMs and hfCFs (figure 1(Ai)). The GelMA bioink induced the formation of small beating cell-clusters ($\sim$30 μm) within the first week of culture, with a uniform distribution and minimal changes up to D22. Cells incorporated in GelMA-matrigel showed larger beating clusters ($\sim$60–100 μm) uniformly distributed throughout the hexagonal microstructures.

Figure 1. *In vitro* hydrogel selection for the myocardial bioink (Myo_B). (A) Brightfield and immunofluorescent staining images of iPSC-CM/hfCF cocultures in the three candidate hydrogels for the myocardial bioink. (i) Brightfield images were taken on D22 of culture. $n = 3$. Representative image shown. Immunofluorescent stainings were performed on D22 of culture using cell-specific antibodies; cardiac troponin T (cTnT) in red to identify and visualize iPSC-CMs and vimentin in green to label fibroblasts. (ii) cTnT channel is shown in isolation to focus on the cardiomyocytes and (iii) shows an overlay of all channels. Scale bar $= 100\ \mu$m. $n = 3$. Representative image shown. Dashed line indicates MEW fiber position. (B) Beating rate analysis of constructs on D4, D7 and D22 of culture. $n = 3$. (C) Mass swelling ratio and (D) soluble fraction analysis of candidate hydrogels. $n = 6$.

GelMA-collagen exhibited cellular rearrangement into a tissue-like structures across the long axis of the hexagons (figure 1(Ai)). These tissue-like structures contracted uniformly and flexed the PCL mesh

(supplementary videos 1–3). Additionally, GelMA-collagen showed iPSC-CMs elongation, cell–cell connection, and bundle formation across the hexagon long axis ($\sim$600 μm) as can be seen by the cardiac

troponin T labeling (figure 1(Aii)). Constructs initially displayed unsynchronized single cell contraction (D2), followed by cluster-like contractions (D4–7). However, only the GelMA-collagen constructs ultimately developed connected and synchronous beating of the entire scaffold. This indicated enhanced cell re-arrangement and connectivity when compared to other bioinks. Furthermore, both the absence of external electrical stimuli (pacing) and the beating rate slowing from D4 to D22 is indicative of reduced self-depolarization, a hallmark of iPSC-CMs maturation. To better understand the relation between gel properties and cell performance, additional analysis was performed on the three gel candidates to determine swelling and soluble fraction. GelMA-collagen had significantly increased mass swelling ratio, as well as soluble fraction (∼2-fold), compared to the other gel candidates (figures 1(C) and (D)), indicative of a lower proportion of crosslinked bonds. Based on the findings of enhanced cellular alignment, iPSC-CM elongation and coordinated beating rate, GelMA-collagen was selected as the optimal hydrogel formulation for the myocardial bioink (Myo_B).

Initially, HUVECs were combined with iPSC-CMs and hfCFs and incorporated in the myocardial bioink, however the mere combination did not result in pre-vascular tissue formation, based upon morphological analysis. Therefore, a separate vascular bioink was developed that supported pre-vascularization and could be extruded sequentially with the cardiac bioink in a controlled vascular-inspired structure. HUVECs and hfCFs were embedded in two bioinks based upon the optimized myocardial bioink with added fibrinogen for functionality and varying photoinitiator concentrations for consequently varied crosslinked density and stiffness (Vasc_B Soft and Vasc_B Stiff). Their ability to form a vascular network was surveyed over a culture period of 14 d using live cell tracking. At D4, HUVECs seeded in Vasc_B Stiff were elongated, and it was possible to observe initial cell–cell contact, whereas Vasc_B Soft exhibited smaller and sparse cells (figure 2(A)). On D7, HUVECs seeded in the Vasc_B Stiff showed thickening of the vessel-like structures with the presence of denser vascular regions that further developed into elongated structures on D14. In the softer bioink, cells were disconnected and clustered around the PCL meshes on D7, which finally collapsed at D14 (figure 2(A)). Quantification of the vascular network showed Vasc_B Stiff to have an approximately 1.5-fold increase in average vessel length with a similar trend for averaging branching length. Additionally, the number of segments increased by approximately three-fold for Vasc_B Stiff in comparison to Vasc_B Soft (figure 2(B)). On D7, the constructs showed the formation of a monolayer-like structure in Vasc_B Soft with extensive αSMA expression with some CD31 colocalization. In Vasc_B

Stiff, vessel-like structures were present with clear CD31 and αSMA colocalization in a 3D structure (figure 2(C)). Based on the findings of improved formation of vessel-like structures, confirmed both with microscopy and quantified vessel length, the Vasc_B stiff hydrogel was selected for use in the vascular bioink (Vasc_B).

Whilst selection of the optimal hydrogel formulations for Myo_B and Vasc_B was primarily based on *in vitro* performance; it was equally important to determine the applicability of EBB deposition into MEW meshes and subsequent optimization of the printing parameters. Printability analysis of hydrogels first included an assessment of the effect on minimum interfilament distance and filament diameter as a result of gel composition and processing temperature at the minimum extrusion pressure (supplementary figure 3). EBB pathways for interfilament fusion (supplementary figure 3(A)) and filament diameter (supplementary figure 3(B)) were adapted from previous literature on gel printability standards [30]. It was observed that temperature increase resulted in a trend of increased filament diameter of all three myocardial gel candidates (supplementary figure 3(D)). This trend was also observed in the analysis of minimum interfilament distance with lower temperatures being associated with the lower interfilament distances possible (supplementary figure 3(C)). As expected, there was a positive correlation observed between filament diameter and the minimum interfilament distance across all three hydrogels (supplementary figure 3(E)), with the highest correlation seen in the GelMA-collagen hydrogel with a $R^2 = 0.9269$ (supplementary figure 3(Eii)).

Whilst the filament formation behavior (supplementary figure 3) confirmed the ability to print with sufficient shape fidelity at different temperatures, it is necessary also to examine the ability of the bioinks to integrate with the MEW mesh (figure 3(A)). To do this, the efficacy of controlled filling of hexagonal pores within the previously defined range was examined using the minimum extrusion pressure to reduce shear stress to the encapsulated cells in the bioinks. Based on these results the quantification of hexagonal pore filling was performed using the path illustrated (figure 3(B)) and minimal pressure for continuous filament formation was recorded for each gel candidate at 10 °C, 12.5 °C and 15 °C (figures 3(C) and (D)). Mesh filling measurements showed considerable variability within most groups and resulted in limited differences when comparing the different extrusion temperatures within each gel candidate group. GelMA printing at 10 °C and 15 °C exhibited an eight-fold increase in percentage filling for the latter, suggesting that the pore-filling percentage and the increase in temperature are correlated. Inversely, the minimum extrusion pressure required for continuous filament formation tended to decrease as the processing temperature
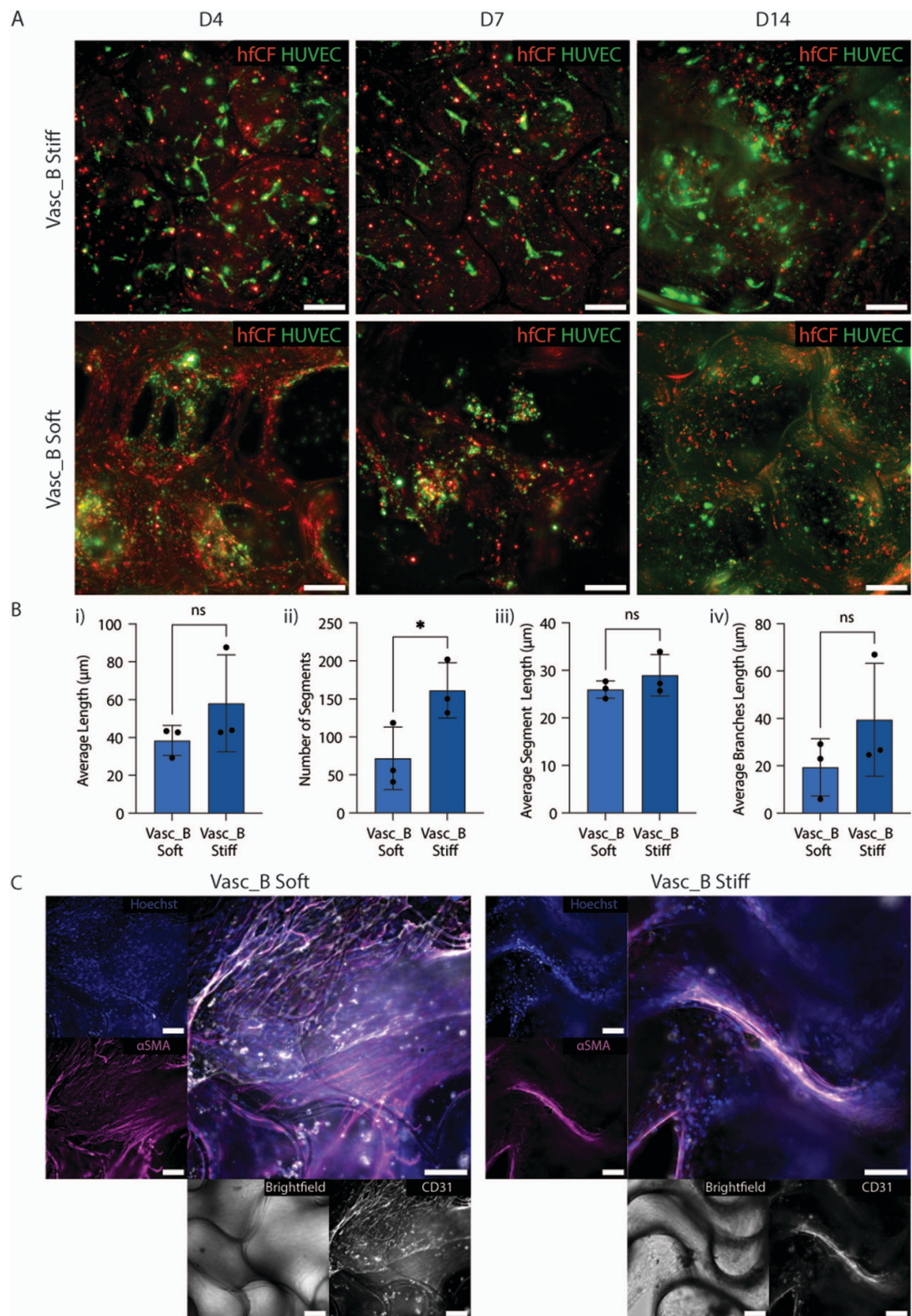
Figure 2. *In vitro* hydrogel selection for the vascular bioink (Vasc_B). (A) Immunofluorescent cell-tracker live images of HUVEC/hfCF cocultures in two candidate hydrogels for the vascular bioink at different timepoints. $n = 3$. Representative image shown of the same samples in time. Scale bar $= 200\ \mu$m. (B) Analysis of vascular network on D7 using Angiogenesis Analyzer with quantifications of (i) average total length, (ii) total number of segments, (iii) average segment length, and (iv) average branches length (segment branching from a main). $N = 3$. Data shown as individual values and mean $\pm$ standard deviation. * $p < 0.05$. (C) Immunofluorescent stainings were performed on fixed samples from D7 of culture and were labeled with cell-specific antibodies; anticlockwise nuclei (Hoechst) in blue, alpha-smooth muscle actin (αSMA) in purple to identify and visualize HUVEC and activated hfCFs, brightfield to visualize the MEW fibers, and CD31 in white to identify HUVEC. Overlayed image of all channels (excluding brightfield) is shown in the central panel. Scale bar $= 100\ \mu$m. $n = 3$. Representative images are shown.

Figure 3. (A) Representation of EBB printing into MEW mesh with expected outcomes based on polymeric/cross-linked density of hydrogel. (B) Schematic overview for EBB path quantification of hexagonal pore filling. (C) Assessment of efficacy of hexagonal mesh filling. $n \geqslant 3$. (D) Minimum feed rate required for extrusion of candidate hydrogels. $n \geqslant 3$. Red dashed line indicated upper limit for acceptable minimum extrusion pressure regarding cell viability. (E) Schematic overview for EBB path to fill the entire construct. (F) Representative image of each candidate hydrogel extruded into MEW mesh filling 1 layer (1L; $n \geqslant 3$, representative image shown) and 3 layers (3L; $n = 3$, representative image shown) using 15 °C processing temperature. Scale bar = 2 mm. (G) Representative image of mesh filling achieved with optimized extrusion pressure (<0.2 bar).

increased whereas only the GelMA-collagen 10 °C and 15 °C differed by three-fold.

Furthermore, rheological analysis (supplementary figure 6) revealed shear thinning behaviors of the three candidate hydrogels. The optimal processing temperature for EBB was 15 °C for all gel compositions due to the balance of extrusion at a low pneumatic pressure, whilst still maintaining enough structural integrity to form filaments, and was henceforth used for entire mesh filling analysis. Upon printing in a programmed pattern (figure 3(E)) that ensured all hexagonal pores to be filled, varied filling proportions were observed between the three candidate hydrogels (figure 3(F)). It was determined that

printing three layers (3L) would ensure the highest percentage of filling before an overflow of hydrogel from the MEW construct occurred. After one layer (1L), the GelMA-collagen candidate was extruded at the most consistent level in each row of hexagons. This observation was continued after three layers, whereas GelMA alone appeared to have some limitations with accuracy of deposition as can be observed by the irregular gel accumulation pattern in one layer. This was furthermore observed after three layers of extrusion, with approximately 60% of the construct filled sufficiently and the remaining mesh filled irregularly. Juxtaposing this, extrusion of GelMA-matrigel exhibited higher regularity, however, displayed a

Figure 4. EBB viability of myocardial (Myo_B) and vascular (Vasc_B) bioinks. (A) Live/dead imaging of cast and printed (using EBB) myocardial and vascular bioinks on D1 and D7 of culture. Green indicated live cells, stained positive using calcein-AM, and red indicates dead cells, stained positive with ethidium homodimer-1. Channels are overlayed. Scale bars = 150 μm. $n = 1$. Representative image of sample shown. (B) Quantification of live/dead assay comparing dead number of cells, normalized against live cell area between printed and casted groups on D1 and D7 of culture. $n > 3$. (C) Metabolic resazurin assay performed on cast and printed (using EBB) myocardial and vascular bioinks on D1, D3 and D7 of culture. Data presented is the mean metabolic activity of printed samples as a percentage against the mean recorded metabolic activity of cast samples. The 100% marking on graph indicates value if metabolic activities of printed and cast samples are identical. $n = 4$.

lower efficacy for filling (supplementary figure 4). After three layers of extrusion, this limitation was subsided with a filling pattern comparable to that of GelMA-collagen.

GelMA-collagen was assessed to be a suitable hydrogel for use in the EBB process, which also best facilitated cardiomyocyte reorganization in the 3D environment and was therefore the selected gel candidate for the myocardial bioink (Myo_B). In line with the results of vascular gel *in vitro* optimization and printability analysis, GelMA-collagen with a stiffer crosslinked network ($2\times$ [photo-initiator]) was selected for the vascular bioink (Vasc_B). Further printability analysis was not carried out as the assumption was made that the photoinitiator concentration should not influence hydrogel properties prior to light exposure, which is the case for the EBB set-up. Subsequent analyses explored the dual-EBB process and implementation of the vascular pathway design.

3.2. Convergence of dual-EBB and MEW
EBB investigations allowed for controlled bioink deposition, thus ensuring cell patterning. The viability of myocardial and vascular bioinks was analyzed after extrusion and compared to casted samples (figure 4). For Myo_B, limited cell death was

observed in both the cast and printed conditions. Quantification of dead cells, normalized against the area of live cells, revealed an elevated but not statistically significant proportion of dead cells of the cast group compared to the printed group in Myo_B (figure 4(B)). An approximate 20% reduction in metabolic activity of the printed group was found as compared to that of the cast group at D1, which further decreased to ∼50% at D7 (figure 4(C)). Reduced metabolic activity was accompanied by hydrogel disc shrinkage and subsequent loss of cells in both groups (data not shown). Despite the lowered metabolic readings at D7, the cells in Myo_B were more elongated, and the discs were observed to contract with synchroneity, indicating a preserved functionality in both conditions (figure 4(A)). Vasc_B showed comparable results in live/dead analysis between cast and printed samples (figure 4(A)). The quantified viability of Vasc_B also showed no significant difference between the cast and printed samples at both D1 and D7 (figure 4(B)). Furthermore, a ∼20% reduction in metabolic activity of the printed group, compared to that of the cast group, was measured on D1, and a fast, sustained recovery after D3 was observed (figure 4(C)). Unlike the Myo_B groups, observed hydrogel disc shrinkage and consequent increased
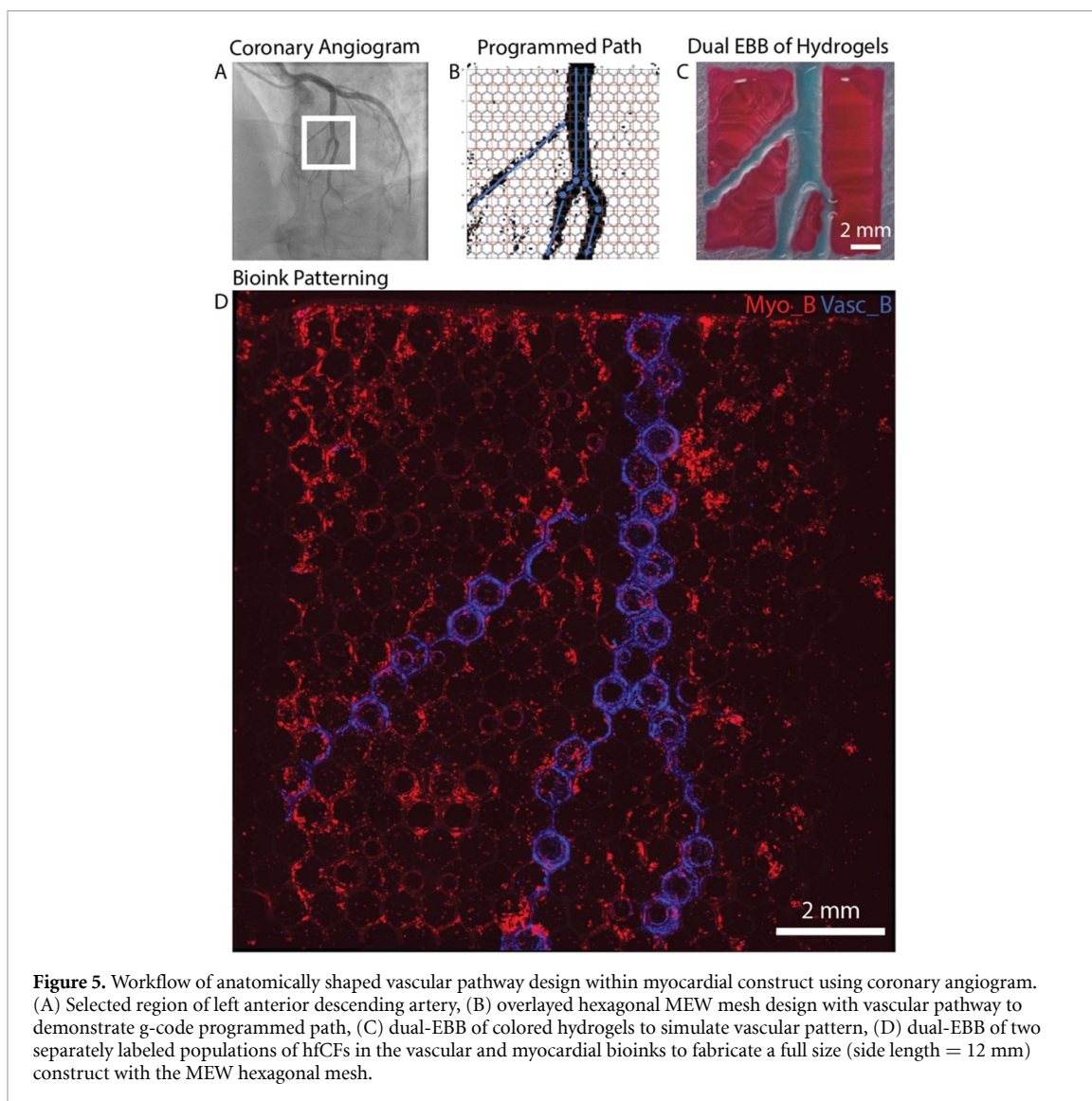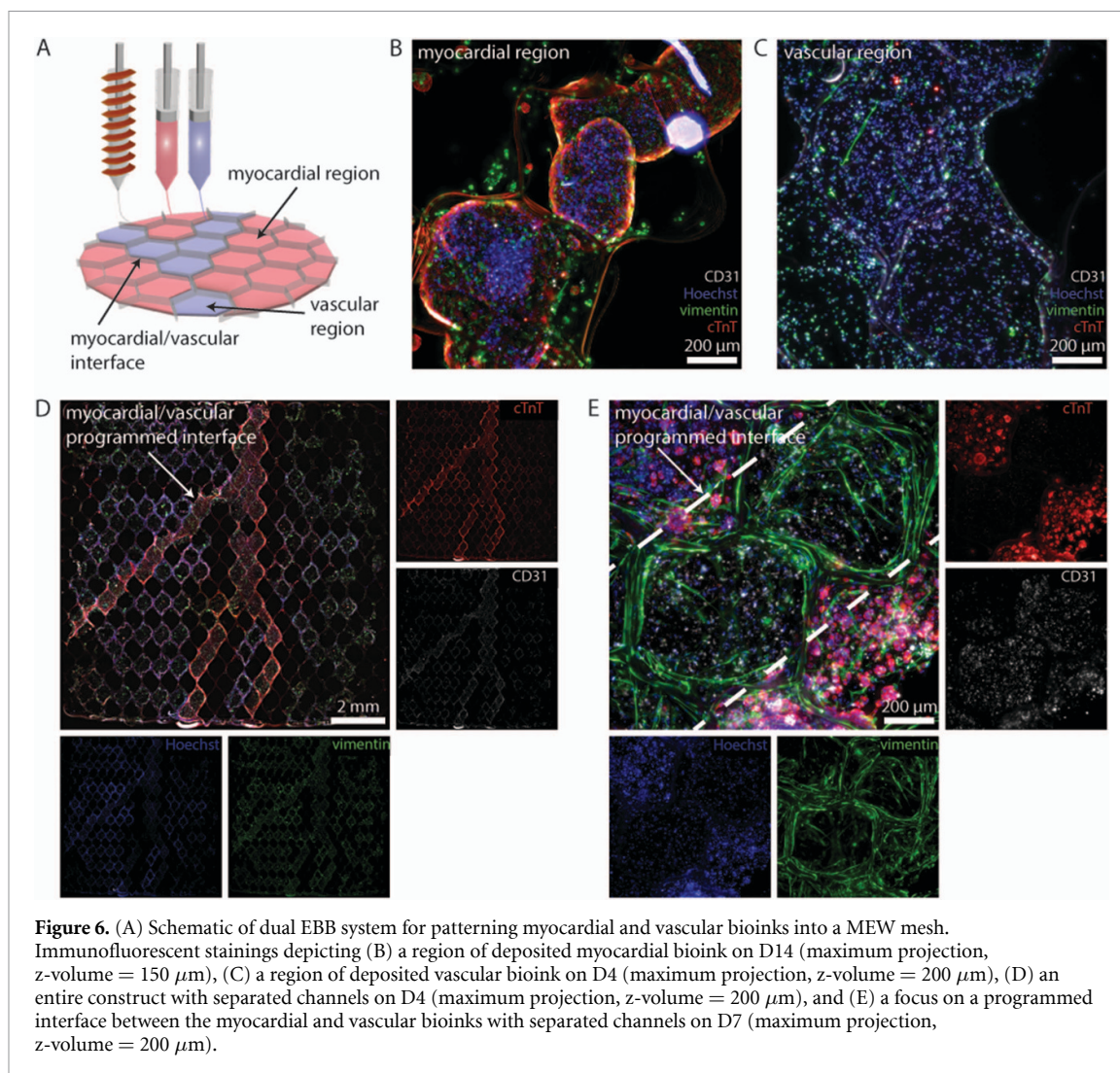
Figure 5. Workflow of anatomically shaped vascular pathway design within myocardial construct using coronary angiogram. (A) Selected region of left anterior descending artery, (B) overlayed hexagonal MEW mesh design with vascular pathway to demonstrate g-code programmed path, (C) dual-EBB of colored hydrogels to simulate vascular pattern, (D) dual-EBB of two separately labeled populations of hfCFs in the vascular and myocardial bioinks to fabricate a full size (side length = 12 mm) construct with the MEW hexagonal mesh.

density correlated positively with increased metabolic activity.

3.3. Fabrication of the pre-vascularized myocardial construct

Next, we further evaluated if the developed Myo_B and Vasc_B bioinks allowed control over myocardial and vascular patterning in a large construct (12 × 12 mm). For this work, a section of the LAD artery was selected from a normal coronary arteriogram [31] (figure 5(A)) and an EBB printing path was programmed (figure 5(B)), resulting in successful printing of two hydrogels, separately colored with different dyes (figure 5(C)). Additionally, separately labeled hfCF populations were extruded, according to the vascular patterned myocardium, into a MEW mesh to fabricate an EHT construct (figure 5(D)). Notably, cells remained localized to the regions where they were printed into and presented an affinity to the MEW fibers in the mesh.

Subsequently, we showed the controlled deposition of two bioinks optimized for vascular (Vasc_B Stiff) and myocardial (GelMA-collagen) tissue formation inside a force-bearing hexagonal PCL mesh (figure 6(A)). On D4 it was observed that the encapsulated cells remained spatially where they were initially extruded (figure 6(D)). Furthermore, on D7 it was possible to observe the formation of a clear interface between the vascular region and the myocardium tissue across two hexagons with endothelial cells branching into the myocardial region, indicating the possibility for endothelial cells to migrate and vascularize (figure 6(E)). Both the separate myocardial (figure 6(B)) and vascular (figure 6(C)) regions could be traced back and identified using cell-specific immunofluorescent labels up to D14. This demonstrated it was possible to ensure controlled colocalization of specialized cells in optimized printable hydrogels, without hindering their specialized functionality and whilst maintaining the ability to undergo organization into tissue-like structures.

Figure 6. (A) Schematic of dual EBB system for patterning myocardial and vascular bioinks into a MEW mesh. Immunofluorescent stainings depicting (B) a region of deposited myocardial bioink on D14 (maximum projection, z-volume = 150 μm), (C) a region of deposited vascular bioink on D4 (maximum projection, z-volume = 200 μm), (D) an entire construct with separated channels on D4 (maximum projection, z-volume = 200 μm), and (E) a focus on a programmed interface between the myocardial and vascular bioinks with separated channels on D7 (maximum projection, z-volume = 200 μm).

4. Discussion

The findings made in this study lay the first steps towards fabricating functional myocardial constructs with pre-vascularization, potentially ensuring, and enhancing anastomotic connection post-implantation. To build upon our previous work where hexagonal MEW scaffolds were utilized to support contracting cardiomyocytes and drive their anisotropic alignment, an anatomically inspired pre-vascular pathway was implemented within the EHT using a combination of both EBB and MEW technology. The convergence of these two technologies also allows for reinforcement of hydrogels to improve the bulk mechanical properties [21] and develop contractile force-enduring constructs that actively support the failing heart.

The first stage of this study involved the optimization of myocardial and vascular bioinks from both functionality and printability points of view. This study aimed to replicate the native myocardium by controlling; firstly, hydrogel polymer network composition, namely its susceptibility to remodeling, and

secondly, deposition of *de novo* ECM from fibroblasts, encouraged by hydrogel degradation. Out of the three gel formations based on GelMA, the addition of collagen proved to result in enhanced cardiomyocyte elongation and formation of tissue-like structures. In our model cardiomyocytes are not electrically stimulated (not paced), and differently from other models [32, 33], their shortening during contraction is unrestrained (isotonic). Thus, the cell rearrangement into larger clusters and ultimately a long, synchronized tissue-like structure was indicative of bioink rearrangement rather than external stimulation. The higher proportion of uncrosslinked polymer in the network likely enabled faster remodeling from the fibroblasts in the co-culture. Initial screening of vascular hydrogel compositions similarly showed the addition of collagen and fibrinogen to the GelMA base was beneficial for vascular cell connectivity. When photoinitiator concentration was to be optimized, it was found that doubling the photoinitiator concentration in the bioink enabled for more stable network connections of the vascular cells, likely due to the mechanical cues required for

these cells to maintain such network formation. This improved vessel-like formation by an increase in matrix stiffness, independently of density, has also been shown previously in collagen-based gels [34, 35]. The higher concentration of photoinitiator in the vascular bioink was assumed to not affect EBB printability since crosslinking is not activated in the process during extrusion and thus, was not investigated as an additional group during the subsequent confirmation for printability.

When confirming the use of the GelMA-collagen hydrogel for EBB, the previously reported printability assays that purely focus on hydrogel deposition [30, 36] were not sufficient on their own to evaluate the convergence of EBB with MEW and did not provide a clear indication of the best performing gel candidate. As such, new methods for assessing EBB integration with MEW meshes were established, measuring the filling of MEW pores, in combination with assessing rheological properties [37]. It was determined that, for this system, viscosity was a key parameter for gel-mesh integration. Markedly, the complex viscosity across the three candidate gels varied in scale, which correlated to the minimum extrusion pressure findings, likely because of the opposing thermal gelation properties of the interpenetrating polymers to the GelMA. It should be noted that this opposing thermal gelation properties, along with the low bioink viscosity and the sensitive set-up of our system, contribute to the overall variability observed throughout the printing fidelity analyses. Whilst this analysis provided valuable insight into predicting gel-mesh integration, it was important to note the variability seen when put into practice. This was especially evident in the GelMA-matrigel group, where varied filling patterns were observed. To overcome this limitation when including cells in the bioink, it was found that repeating the filling pattern three times (3L) allowed for effective filling of the entire mesh without experiencing overflowing of gel from the mesh. We speculate that lowering the collector speed or increasing the pressure could alternatively be applied, yet, this more likely causes local overfilling when material extrusion exceeds the speed of fiber wall wetting/pore filling.

When bioprinting both myocardial and vascular cells in an extrusion-based system, it is important to consider the effect of cellular density and pneumatic pressure on the viability and functionality of the cells [38]. Extrusion pressure was adjusted to <0.2 bar to achieve mesh filling, while minimizing detrimental viability effects, in line with previous work [39]. Whilst there was no marked difference in viability of both bioinks between cast and EBB-printed samples, metabolic activity was upregulated in the vascular bioink and downregulated in the myocardial bioink. An explanation of this could be the lack of structural stability usually provided by the MEW mesh, which was absent in the experimental setup, resulting in a reduction of stability allowing

for accelerated remodeling of the gels by the cells, likely by the hfCFs over the one-week culture period. This was characterized by a shrinking of the gel-cell constructs and resultant increased cellular density. Consequently, quantification of viable cells was unreliable due to overlapping, leading to a measurement of the area of the live cells for normalization of cell death. The confirmation of sustained cell viability post-printing allowed for the development of the patterned pre-vascular pathway. Importantly, this concept is adaptable depending on the location for implantation, considering the vascular fraction and density. Here, a section of the LAD was selected as a proof of concept since it is a commonly occluded coronary vessel. This study exhibited a base model towards producing EHTs with fiber-reinforcing anisotropy and could be further developed into a multiple-layered, organized construct with a pre-vascular bed that can induce sprouting.

Approaches for escalating the formation of pre-vasculature could focus on formation of tubular structures that have sprouting capabilities, including previously investigated techniques, like the use of fishing wire, subcutaneous implantation for vascular ingrowth, sacrificial 3D-printing, tubular solution electrospinning/MEW, and EBB [40–43]. This study demonstrated how convergence of MEW and EBB allows for the development of a cardiac construct with myocardial tissue-like anisotropy and controlled deposition of myocardial and vascular bioinks as a first step to provide construct pre-vascularization. The proposed approach is envisioned to improve tissue anastomosis upon implantation, ultimately increasing integration, survival, and contractile function. Next to the presented construct anisotropy and pre-vascularization, increased thickness has previously been shown to provide enhanced functional outcomes [44–48]. Thus, the desired thickness could be achieved in future works by applying this concept to a series of stacked meshes to achieve cardiomyocyte bundles with directed alignments. Additionally, the ability to control structural and morphological similarity to the organized native tissue alignment can ultimately open up the possibility to personalized tissue engineering based on patient-specific imaging with matched vascular network structure of the specific area to be treated.

5. Conclusion

This study presents the fabrication of a pre-vascularized EHT in which a hexagonal MEW mesh is patterned using a dual EBB approach. This convergence of technologies opens new perspectives in terms of shape fidelity for soft hydrogels across a range of applications. It also demonstrated the possibility to use a mechanically weaker hydrogel, reinforced with MEW fibers, whilst still maintaining locational control over cellular composition, type, and density.

The development of EHTs with myocardial tissue-like formation with a pre-vascular pathway produced using a combination of MEW and EBB has laid the groundwork for the next steps of producing structurally organized, sufficiently thick EHTs that are capable of anastomotic connection with the patient for enhanced functional survival.

Data availability statement

The data cannot be made publicly available upon publication because they are not available in a format that is sufficiently accessible or reusable by other researchers. The data that support the findings of this study are available upon reasonable request from the authors.

Acknowledgments

ORCID iDs

Madison Jade Ainsworth ⓘ https://orcid.org/0000-0002-7768-6392
Nino Chirico ⓘ https://orcid.org/0000-0002-3787-6466
Mylène de Ruijter ⓘ https://orcid.org/0000-0002-8685-8379
Joost P G Sluijter ⓘ https://orcid.org/0000-0003-2088-9102
Jos Malda ⓘ https://orcid.org/0000-0002-9241-7676
Alain van Mil ⓘ https://orcid.org/0000-0001-9906-5047
Miguel Castilho ⓘ https://orcid.org/0000-0002-4269-5889

References

[1] James S L *et al* 2018 Global, regional, and national incidence, prevalence, and years lived with disability for 354 diseases and injuries for 195 countries and territories, 1990–2017: a systematic analysis for the Global Burden of Disease Study 2017 *Lancet* **392** 1789–858

[2] Bergmann O *et al* 2009 Evidence for cardiomyocyte renewal in humans *Science* **324** 98–102

[3] Bergmann O *et al* 2015 Dynamics of cell generation and turnover in the human heart *Cell* **161** 1566–75

[4] He L, Nguyen N B, Ardehali R and Zhou B 2020 Heart regeneration by endogenous stem cells and cardiomyocyte proliferation *Circulation* **142** 275–91

[5] van den Akker F *et al* 2017 Intramyocardial stem cell injection: go(ne) with the flow *Eur. Heart J.* **38** 184–6

[6] Gaetani R, Feyen D A, Verhage V, Slaats R, Messina E, Christman K L, Giacomello A, Doevendans P A F M and Sluijter J P G 2015 Epicardial application of cardiac progenitor cells in a 3D-printed gelatin/hyaluronic acid patch preserves cardiac function after myocardial infarction *Biomaterials* **61** 339–48

[7] Madonna R *et al* 2019 ESC working group on cellular biology of the heart:position paper for cardiovascular research: tissue engineering strategies combined with cell therapies for cardiac repair in ischaemic heart disease and heart failure *Cardiovasc. Res.* **115** 488–500

[8] Schwach V and Passier R 2019 Native cardiac environment and its impact on engineering cardiac tissue *Biomater. Sci.* **7** 3566–80

[9] Kristen M, Ainsworth M J, Chirico N, van der Ven C F T, Doevendans P A, Sluijter J P G, Malda J, Mil A and Castilho M 2020 Fiber scaffold patterning for mending hearts: 3D organization bringing the next step *Adv. Healthcare Mater.* **9** 1900775

[10] Castilho M, van Mil A, Maher M, Metz C H G, Hochleitner G, Groll J, Doevendans P A, Ito K, Sluijter J P and Malda J 2018 Melt electrowriting allows tailored microstructural and mechanical design of scaffolds to advance functional human myocardial tissue formation *Adv. Funct. Mater.* **28** 1803151

[11] O'Brien F J 2011 Biomaterials & scaffolds for tissue engineering *Mater. Today* **14** 88–95

[12] Redd M A, Zeinstra N, Qin W, Wei W, Martinson A, Wang Y, Wang R K, Murry C E and Zheng Y 2019 Patterned human microvascular grafts enable rapid vascularization and increase perfusion in infarcted rat hearts *Nat. Commun.* **10** 584

[13] Liu Y *et al* 2022 hESCs-derived early vascular cell spheroids for cardiac tissue vascular engineering and myocardial infarction treatment *Adv. Sci.* **9** 2104299

[14] de Ruijter M, Ribeiro A, Dokter I, Castilho M and Malda J 2019 Simultaneous micropatterning of fibrous meshes and bioinks for the fabrication of living tissue constructs *Adv. Healthcare Mater.* **8** 1800418

[15] Maiullari F *et al* 2018 A multi-cellular 3D bioprinting approach for vascularized heart tissue engineering based on HUVECs and iPSC-derived cardiomyocytes *Sci. Rep.* **8** 13532

[16] Noor N, Shapira A, Edri R, Gal I, Wertheim L and Dvir T 2019 3D printing of personalized thick and perfusable cardiac patches and hearts *Adv. Sci.* **6** 1900344

[17] Roche C D, Sharma P, Ashton A W, Jackson C, Xue M and Gentile C 2021 Printability, durability, contractility and vascular network formation in 3D bioprinted cardiac endothelial cells using alginate–gelatin hydrogels *Front. Bioeng. Biotechnol.* **9** 636257

[18] Castilho M, de Ruijter M, Beirne S, Villette C C, Ito K, Wallace G G and Malda J 2020 Multitechnology biofabrication: a new approach for the manufacturing of functional tissue structures? *Trends Biotechnol.* **38** 1316–28

[19] Alcala-Orozco C R, Cui X, Hooper G J, Lim K S and Woodfield T B F 2021 Converging functionality: strategies for 3D hybrid-construct biofabrication and the role of composite biomaterials for skeletal regeneration *Acta Biomater.* **132** 188–216

[20] Dufour A, Gallostra X B, O'Keeffe C, Eichholz K, von Euw S, Garcia O and Kelly D J 2022 Integrating melt electrowriting and inkjet bioprinting for engineering structurally organized articular cartilage *Biomaterials* **283** 121405

[21] Melchels F P W, Blokzijl M M, Levato R, Peiffer Q C, MnD R, Hennink W E, Vermonden T and Malda J 2016 Hydrogel-based reinforcement of 3D bioprinted constructs *Biofabrication* **8** 035004

[22] Bas O *et al* 2017 An integrated design, material, and fabrication platform for engineering biomechanically and biologically functional soft tissues *ACS Appl. Mater. Interfaces* **9** 29430–7

[23] Hamad S, Derichsweiler D, Papadopoulos S, Nguemo F, Saric T, Sachinidis A, Brockmeier K, Hescheler J, Boukens B J and Pfannkuche K 2019 Generation of human induced pluripotent stem cell-derived cardiomyocytes in 2D monolayer and scalable 3D suspension bioreactor cultures with reduced batch-to-batch variations *Theranostics* **9** 7222–38

[24] Chirico N *et al* 2022 Small molecule-mediated rapid maturation of human induced pluripotent stem cell-derived cardiomyocytes *Stem. Cell Res. Ther.* **13** 531

[25] Bracco Gartner T C L, Crnko S, Leiteris L, van Adrichem I, van Laake L W, Bouten C V C, Goumans M J, Suyker W J L, Sluijter J P G and Hjortnaes J 2022 Pirfenidone has anti-fibrotic effects in a tissue-engineered model of human cardiac fibrosis *Front. Cardiovasc. Med.* **9** 854314

[26] Bracco Gartner T C L, Stein J M, Muylaert D E P, Bouten C V C, Doevendans P A, Khademhosseini A, Suyker W J L, Sluijter J P G and Hjortnaes J 2021 Advanced *in vitro* modeling to study the paradox of mechanically induced cardiac fibrosis *Tissue Eng.* C **27** 100–14

[27] World Medical Association Declaration of Helsinki 2001 Ethical principles for medical research involving human subjects *Bull. World Health Organ.* **79** 373–4

[28] Melchels F P W, Dhert W J A, Hutmacher D W and Malda J 2014 Development and characterisation of a new bioink for additive tissue manufacturing *J. Mater. Chem.* B **2** 2282–9

[29] Carpentier G, Berndt S, Ferratge S, Rasband W, Cuendet M, Uzan G and Albanese P 2020 Angiogenesis analyzer for ImageJ—a comparative morphometric analysis of "endothelial tube formation assay" and "fibrin bead assay" *Sci. Rep.* **10** 11568

[30] Ribeiro A, Blokzijl M M, Levato R, Visser C W, Castilho M, Hennink W E, Vermonden T and Malda J 2017 Assessing bioink shape fidelity to aid material development in 3D bioprinting *Biofabrication* **10** 014102

[31] Normal coronary angiogram (DSA) 2018 Radiopaedia.org (available at: https://radiopaedia.org/cases/63081)

[32] Cho S, Discher D E, Leong K W, Vunjak-Novakovic G and Wu J C 2022 Challenges and opportunities for the next generation of cardiovascular tissue engineering *Nat. Methods* **19** 1064–71

[33] Tani H and Tohyama S 2022 Human engineered heart tissue models for disease modeling and drug discovery *Front. Cell Dev. Biol.* **10** 855763

[34] Mason B N, Starchenko A, Williams R M, Bonassar L J and Reinhart-King C A 2013 Tuning three-dimensional collagen matrix stiffness independently of collagen concentration modulates endothelial cell behavior *Acta Biomater.* **9** 4635–44

[35] Yamamura N, Sudo R, Ikeda M and Tanishita K 2007 Effects of the mechanical properties of collagen gel on the *in vitro* formation of microvessel networks by endothelial cells *Tissue Eng.* **13** 1443–53

[36] Malda J, Visser J, Melchels F P, Jüngst T, Hennink W E, Dhert W J A, Groll J and Hutmacher D W 2013 25th anniversary article: engineering hydrogels for biofabrication *Adv. Mater.* **25** 5011–28

[37] Paxton N, Smolan W, Böck T, Melchels F, Groll J and Jungst T 2017 Proposal to assess printability of bioinks for extrusion-based bioprinting and evaluation of rheological properties governing bioprintability *Biofabrication* **9** 044107

[38] Kalhori D, Zakeri N, Zafar-Jafarzadeh M, Moroni L and Solati-Hashjin M 2022 Cardiovascular 3D bioprinting: a review on cardiac tissue development *Bioprinting* **28** e00221

[39] Fakhruddin K, Hamzah M S A and Razak S I A 2018 Effects of extrusion pressure and printing speed of 3D bioprinted construct on the fibroblast cells viability *IOP Conf. Ser.: Mater. Sci. Eng.* **440** 012042

[40] Hasan A, Memic A, Annabi N, Hossain M, Paul A, Dokmeci M R, Dehghani F and Khademhosseini A 2014 Electrospun scaffolds for tissue engineering of vascular grafts *Acta Biomater.* **10** 11–25

[41] Jungst T, Pennings I, Schmitz M, Rosenberg A J W P, Groll J and Gawlitta D 2019 Heterotypic scaffold design orchestrates primary cell organization and phenotypes in cocultured small diameter vascular grafts *Adv. Funct. Mater.* **29** 1905987

[42] Pennings I, van Haaften E E, Jungst T, Bulsink J A, Rosenberg A J W P, Groll J, Bouten C V C, Kurniawan N A, Smits A I P M and Gawlitta D 2019 Layer-specific cell differentiation in bi-layered vascular grafts under flow perfusion *Biofabrication* **12** 015009

[43] Tomasina C, Bodet T, Mota C, Moroni L and Camarero-Espinosa S 2019 Bioprinting vasculature: materials, cells and emergent techniques *Materials* **12** 2701

[44] Taylor D A, Sampaio L C and Gobin A 2014 Building new hearts: a review of trends in cardiac tissue engineering *Am. J. Transplant.* **14** 2448–59

[45] Pretorius D, Kahn-Krell A M, Lou X, Fast V G, Berry J L, Kamp T J and Zhang J 2021 Layer-by-layer fabrication of large and thick human cardiac muscle patch constructs with superior electrophysiological properties *Front. Cell Dev. Biol.* **9** 670504

[46] Perea-Gil I, Prat-Vidal C and Bayes-Genis A 2015 *In vivo* experience with natural scaffolds for myocardial infarction: the times they are a-changin' *Stem. Cell Res. Ther.* **6** 248

[47] Zimmermann W H *et al* 2006 Engineered heart tissue grafts improve systolic and diastolic function in infarcted rat hearts *Nat. Med.* **12** 452–8

[48] Zimmermann W H, Melnychenko I and Eschenhagen T 2004 Engineered heart tissue for regeneration of diseased hearts *Biomaterials* **25** 1639–47